

Received:  
04 October 2022

Revised:  
25 April 2023

Accepted:  
24 May 2023

© 2023 The Authors. Published by the British Institute of Radiology under the terms of the Creative Commons Attribution 4.0 Unported License <http://creativecommons.org/licenses/by/4.0/>, which permits unrestricted use, distribution and reproduction in any medium, provided the original author and source are credited.

Cite this article as:

Woodward OB, Driver I, Schwarz ST, Hart E, Wise R. Assessment of brainstem function and haemodynamics by MRI: challenges and clinical prospects. *Br J Radiol* (2023) 10.1259/bjr.20220940.

## REVIEW ARTICLE

# Assessment of brainstem function and haemodynamics by MRI: challenges and clinical prospects

<sup>1</sup>OWEN BLEDDYN WOODWARD, MPhys MBBCh FRCR, <sup>1</sup>IAN DRIVER, MSc PhD, <sup>1,2</sup>STEFAN THEODOR SCHWARZ, PhD MD MSc FRCR EDINR, <sup>3</sup>EMMA HART, BSc PhD and <sup>1,4,5</sup>RICHARD WISE, MA, PhD

<sup>1</sup>Cardiff University Brain Research Imaging Centre (CUBRIC), Cardiff University, Cardiff, United Kingdom

<sup>2</sup>University Hospital of Wales, Cardiff, United Kingdom

<sup>3</sup>University of Bristol, Bristol, United Kingdom

<sup>4</sup>Institute for Advanced Biomedical Technologies, University "G. d'Annunzio" of Chieti-Pescara, Chieti, Italy

<sup>5</sup>Department of Neurosciences, Imaging and Clinical Sciences, University "G. d'Annunzio" of Chieti-Pescara, Chieti, Italy

Address correspondence to: Owen Bleddyn Woodward  
E-mail: [WoodwardO@cardiff.ac.uk](mailto:WoodwardO@cardiff.ac.uk)

## ABSTRACT

MRI offers techniques for non-invasively measuring a range of aspects of brain tissue function. Blood oxygenation level dependent (BOLD) functional magnetic resonance imaging (fMRI) is widely used to assess neural activity, based on the brain's haemodynamic response, while arterial spin labelling (ASL) MRI is a non-invasive method of quantitatively mapping cerebral perfusion. Both techniques can be applied to measure cerebrovascular reactivity (CVR), an important marker of the health of the cerebrovascular system. BOLD, ASL and CVR have been applied to study a variety of disease processes and are already used in certain clinical circumstances. The brainstem is a critical component of the central nervous system and is implicated in a variety of disease processes. However, its function is difficult to study using MRI because of its small size and susceptibility to physiological noise. In this article, we review the physical and biological underpinnings of BOLD and ASL and their application to measure CVR, discuss the challenges associated with applying them to the brainstem and the opportunities for brainstem MRI in the research and clinical settings. With further optimisation, functional MRI techniques could feasibly be used to assess brainstem haemodynamics and neural activity in the clinical setting.

## INTRODUCTION

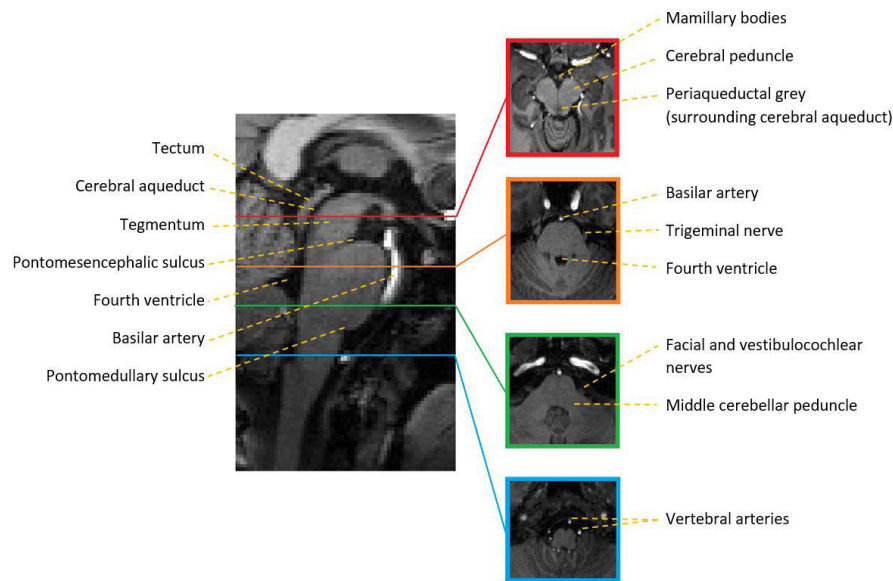
The brainstem serves as a conduit for ascending and descending nerve tracts and it contains cranial nerve nuclei as well as autonomic centres that control blood pressure, heart rate and respiration. It is a critical element of the central nervous system, but it is more challenging to study using magnetic resonance imaging (MRI) than many other regions of the brain. While routine clinical MRI usually aims to identify structural abnormalities, MRI is also capable of non-invasively interrogating the function of the central nervous system. Blood oxygenation level dependent (BOLD) functional MRI (fMRI) is a method of assessing neuronal function, and arterial spin labelling (ASL) is a non-invasive method of assessing cerebral perfusion without the administration of an exogenous contrast agent. Both ASL and BOLD can also be used to measure cerebrovascular reactivity (CVR), an important marker of the health of the cerebrovascular system.

The application of these techniques to evaluate the brainstem is largely confined to research at the moment, but brainstem networks involved in pain processing,<sup>1,2</sup> arousal<sup>3,4</sup> and autonomic activity<sup>5-8</sup> have been mapped to various extents. The increasing availability of 3 Tesla scanners may open the door to the future clinical application of brainstem fMRI. This review is aimed at clinicians who are interested in applying functional MRI methods in their clinical or research practice to examine patterns of changing neuronal activity in the brainstem and assess haemodynamic function. We introduce the technical details underpinning the techniques and their availability, discuss the challenges associated with applying them to the brainstem and describe the future potential for applying brainstem functional MRI in the clinical setting.

## FUNCTIONAL NEUROANATOMY OF THE BRAINSTEM

The brainstem is a small structure<sup>9</sup> consisting of three regions, the midbrain, pons and medulla (Figure 1). The

Figure 1. Brainstem anatomy outlined on  $T_1$ -weighted mid-sagittal and selected axial cross-sections through the brainstem.



average diameter of its smallest subdivision, the medulla, is 14 mm<sup>10</sup> and many brainstem nuclei measure less than 1 mm in diameter<sup>11,12</sup>. The cerebral aqueduct runs through the midbrain, connecting the third and fourth ventricles and separating the midbrain into the tectum dorsally, and the tegmentum and cerebral peduncles, which connect the midbrain to the cerebral hemispheres, ventrally. Notable structures within the midbrain include the substantia nigra (involved in reward and movement), the red nucleus (also involved in motor coordination), and the periaqueductal grey (involved in pain processing). Cranial nerves III and IV arise from the midbrain surface. The inferior boundary of the midbrain is defined by the pontomesencephalic sulcus. Below this lies the pons, the largest subdivision. The ventral pons contains motor nuclei which communicate with the cerebellum via the middle cerebellar peduncle. Dorsally, the phylogenetically older tegmentum houses parts of the reticular formation (involved in arousal and wakefulness). The trigeminal nerve (cranial nerve V) arises from the pons. Cranial nerves VI, VII and VIII arise from the pontomedullary sulcus, which defines the boundary between the pons and medulla. This is the most caudal subdivision of the brainstem, and it merges with the spinal cord inferiorly. The pyramids, which contain motor fibres from the prefrontal cortex, decussate in the ventral medulla, and cranial nerves IX, X, XI and XII emerge from its surface. While the precise anatomy of the brainstem vasculature is somewhat variable,<sup>13</sup> most of the arterial supply to the brainstem is from the vertebrabasilar arteries.

## ARTERIAL SPIN LABELLING

### Physical principles

ASL involves magnetically 'labelling' the water in a bolus of intravascular blood, which then travels into the brain parenchyma enabling an estimation of perfusion to be made through the application of a kinetic model.<sup>14</sup> A radiofrequency inversion pulse is applied to invert the magnetisation of blood in the carotid and vertebral arteries, then after a short time delay (termed the post-label delay (PLD)) to allow it to travel to the brain, a 'tag'

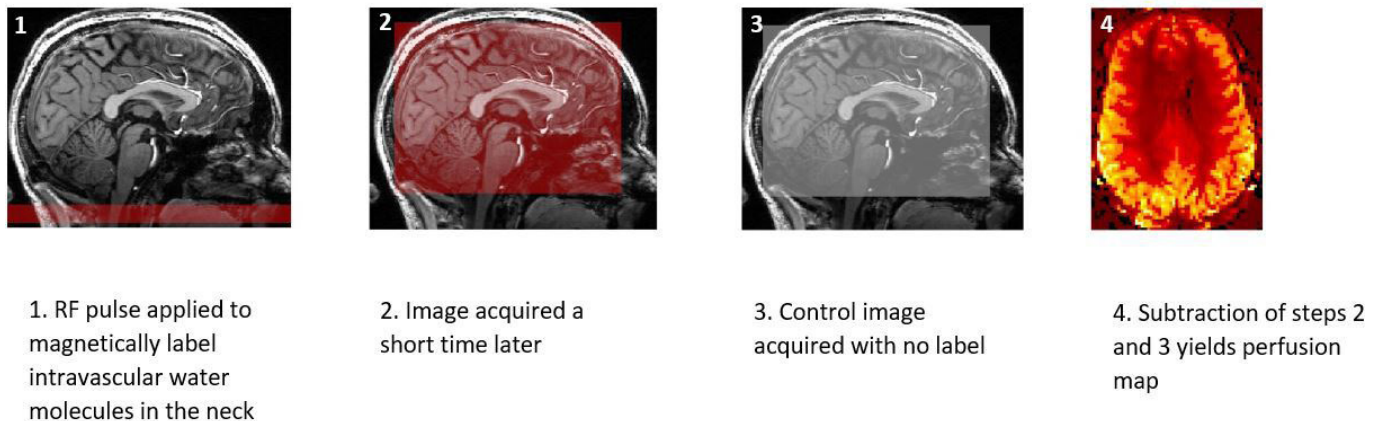
image is acquired. A 'control' image is then acquired, identical to the 'tag' image in all respects apart from the inversion effect of the labelling pulse. Subtraction of the 'tag' and 'control' images ideally leaves only signal from inverted blood, which represents perfusion information (Figure 2).

There are two main labelling techniques which are currently in use. Pseudocontinuous ASL (PCASL) involves the application of a train of radiofrequency (RF) pulses together with a magnetic field gradient (applied in the direction of blood flow). As blood flows along the field gradient, the precession frequency of hydrogen nuclei sweeps through resonance with the applied RF pulse. The alternate approach, pulsed ASL, involves the application of a single RF pulse to the labelling volume which almost instantaneously inverts the net magnetisation within that volume. The details of these techniques can be found in previous publications.<sup>15,16</sup>

In order to achieve efficient inversion of blood as it flows through the labelling plane, it is important to apply the labelling pulse perpendicular to the direction of blood flow in the arterial vessels of the neck. This is especially important for brainstem ASL because of the tortuous course of the vertebral arteries in the superior part of the neck (Figure 3). An angiogram can be acquired to help locate the labelling plane (Figure 3).<sup>15</sup> An alternative labelling method, velocity-selective ASL (VSASL), involves labelling blood according to its flow velocity rather than its spatial location.<sup>17</sup> Blood within arterioles supplying the brain parenchyma can therefore be directly labelled. This helps to reduce the signal decay during transit and is less sensitive to the confounding effects of pathology that involves slow or collateral blood flow. The disadvantage of VSASL is that SNR is generally slightly lower than PCASL, and label flow velocity must be accurately targeted.<sup>18</sup>

The magnitude of the difference in signal between the "tag" and "control" images is of the order of 1% of the static tissue water

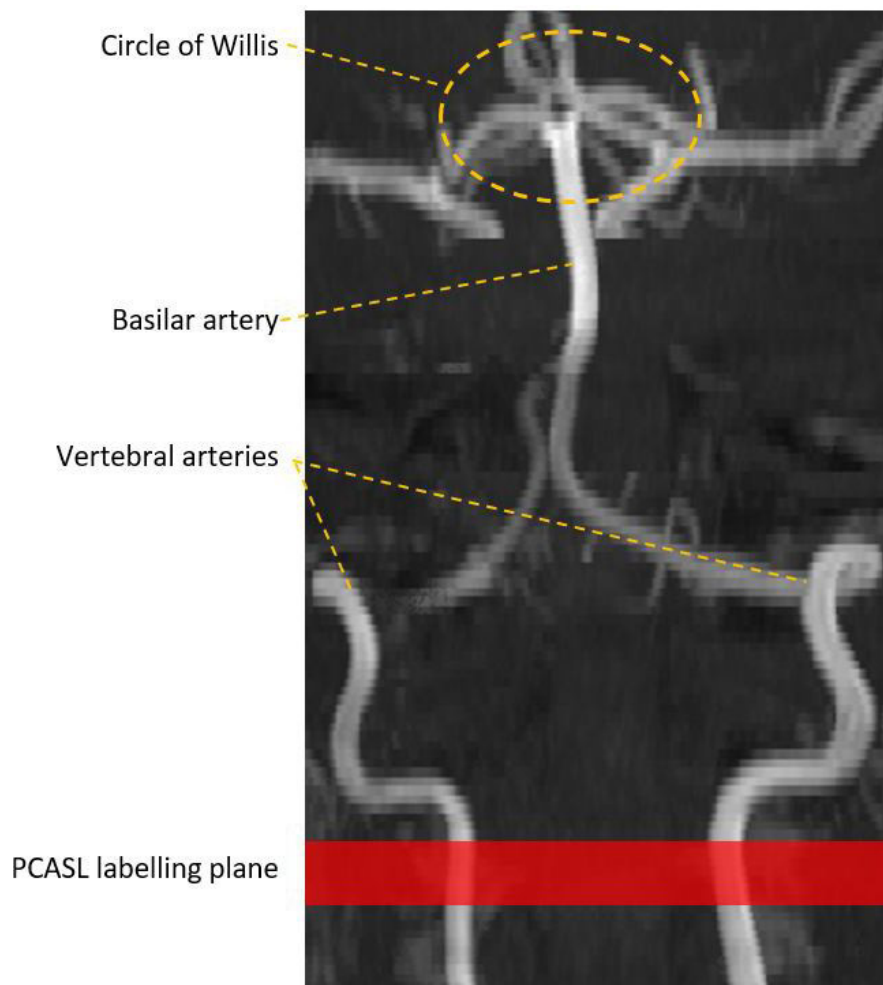
Figure 2. Simplified representation of step-by-step process of generating a cerebral perfusion map using arterial spin labelling.



signal.<sup>15</sup> ASL is, therefore, an inherently low SNR technique. Any form of motion (head movement, physiological tissue displacements or distortions due to noise) between the acquisition of tag and control pairs will have a significant detrimental effect on SNR.<sup>19</sup> Unfortunately, the brainstem is especially susceptible

to such sources of noise, as discussed below. The magnitude of the signal due to such sources of variation is proportional to the signal in the background (unsubtracted) images and is, therefore, potentially much greater than the perfusion signal. Background suppression aims to minimise the signal that originates from

Figure 3. Time-of-flight MRI angiogram of the vertebrobasilar arteries demonstrating representative example of label location for brainstem ASL.



static tissues, therefore reducing the effects of any such tissue motion in the image and improving the SNR of the final perfusion image. Background suppression is performed by applying a series of inversion pulses before the acquisition of each image volume. However, the technique is less than 100% efficient and can reduce by as much as 5% the ASL signal.<sup>15</sup> Post-processing techniques such as motion correction can also be applied, but good patient compliance within the scanner is especially important for obtaining good quality data at the outset.

The time it takes for blood to travel from the labelling plane to brain tissue is known as the arterial transit time (ATT), while the time between labelling and imaging readout is termed the post-labelling delay (PLD). If the PLD is too short, labelled blood might still reside within the basilar artery, which lies in close opposition to the pons, confounding CBF measurements. The PLD needs to be long enough to allow the labelled blood bolus to perfuse into brain tissue. However, the labelled signal decays with T1 relaxation, so longer PLDs reduce the measurement sensitivity and increase acquisition time. Therefore, a PLD that is slightly longer than the longest ATT is recommended<sup>15</sup> so that most of the labelled blood has reached the cerebral microvasculature before the 'tag' image is acquired.

ATT is likely to vary somewhat between individuals, due to variations in flow dynamics and vascular anatomy, or due to vascular pathology.<sup>20</sup> Ideally, the PLD would be tailored to each individual participant according to their ATT. Multi-PLD ASL involves acquiring ASL data at multiple delay times and enables the kinetic curve of the labelled water to be modelled. This approach allows an ATT to be estimated and used to generate perfusion values which are less sensitive to differences in ATT between brain regions and individuals.<sup>21</sup> However, multi-PLD ASL SNR is generally lower because fewer tag-control pairs can be acquired per unit time compared to single-PLD acquisitions.<sup>15</sup>

The intrinsic SNR of ASL is higher at 3T than 1.5 T, and T1 relaxation time is longer, enabling a sufficiently high resolution to delineate regional perfusion differences in the brainstem. Brainstem ASL is, therefore, much more technically feasible in the clinical setting with the increasing prevalence of 3T scanners.

### Applications

ASL has not yet achieved widespread application in the clinical setting. However, it offers a potentially useful alternative to techniques that involve ionising radiation such as CT and PET.<sup>15</sup> In acute stroke, CT perfusion or dynamic susceptibility contrast (DSC) MR<sup>22</sup> can be used to delineate areas of potentially salvageable brain tissue to select candidates for mechanical thrombectomy. ASL has been shown to be comparable to DSC MR methods.<sup>23-25</sup> A typical single-PLD ASL acquisition is quick (taking approximately 5 min) and can generate a map of relative cerebral blood flow capable of demonstrating within-subject regional perfusion differences, without the need for complex post-processing methods. ASL could, therefore, serve as part of a standard neuroimaging protocol in assessing patients presenting with symptoms of acute ischaemic stroke. The sensitivity of ASL techniques to pathology that affects the arterial transit time, such

as arterial occlusion or stenosis that occurs in ischaemic stroke, can also be exploited to identify collateral supply to hypoperfused regions. Residual labelled blood within the macrovascular circulation will be identified in these areas on perfusion maps as hyperintensities not conforming to the expected distribution of brain perfusion. ASL is potentially more sensitive than time-of-flight MR angiography in detecting arteriovenous malformations and shunts because of the high concentration of labelled blood that flows through these malformations.<sup>26</sup>

ASL is a useful alternative to DSC MRI in assessing the haemodynamics of primary and metastatic brain tumours.<sup>26</sup> ASL-derived CBV maps can aid in differentiating between low and high-grade tumours, as well as being useful in post-treatment surveillance for high-grade transformation. CBV maps are also useful in differentiating disease progression and response from treatment-related changes (pseudoprogression and pseudoreponse, respectively).<sup>27</sup> ASL does not require vascular access or intravenous contrast administration, which is especially desirable in the paediatric population where there is uncertainty surrounding the potential long-term effects of gadolinium accumulation in the brain.<sup>23,28</sup>

Cerebral perfusion and metabolism have been shown to be coupled,<sup>29</sup> and ASL could be an adjunct to PET in identifying reductions in cerebral perfusion or metabolism in early Alzheimer's disease.<sup>26</sup> It is also capable of identifying perfusion alterations at epileptogenic foci,<sup>30</sup> even in the absence of structural abnormalities.

So far ASL has predominantly been applied to study cortical perfusion. However, the feasibility of measuring regional brainstem perfusion at 3T has been demonstrated, and brainstem ASL has been applied in various research settings. These include the demonstration of differential effects of methylphenidate and atomoxetine on regional CBF, including the midbrain,<sup>31</sup> the study of CBF changes in neonates with hypoxic ischaemic encephalopathy<sup>32,33</sup> and in differentiating between hereditary ataxia and spastic paraplegia.<sup>34</sup> With the increasing availability of high-field 3 Tesla MRI in the clinical setting, the applications of ASL described above could all feasibly be applied in the brainstem, and the main vendors are able to supply one or more of the described variants of ASL sequences on the MRI systems that they offer.

## BOLD FUNCTIONAL MAGNETIC RESONANCE IMAGING

### Physical principles

Blood oxygen level dependent (BOLD) fMRI is based on localised temporal variation in MRI signal due to changes in local concentrations of deoxyhaemoglobin in brain tissue. Oxygenated haemoglobin in the arterial circulation is diamagnetic. Conversely, deoxyhaemoglobin, that is found in higher concentration on the venous side-of the circulation, is paramagnetic and induces local static magnetic field inhomogeneities which lead to accelerated MRI signal decay caused by a loss of phase coherence (T2\* relaxation). Increased neuronal activity leads to increased cerebral blood flow (CBF) in the local capillary

network via a process known as neurovascular coupling.<sup>35</sup> The fractional increase in CBF exceeds the fractional increase in tissue demand for oxygen (cerebral metabolic rate of oxygen consumption or CMRO<sub>2</sub>), and therefore, somewhat counterintuitively, the oxygen extraction fraction (OEF) from the arterial circulation is lower in regions of higher metabolic activity than in less metabolically active regions. Therefore, in metabolically active regions, the relative concentration of deoxyhaemoglobin is lower, T2\* relaxation time is prolonged, and the MRI signal is increased,<sup>14</sup> normally marking an increase in neuronal activity.

The BOLD signal arises from the haemodynamic response to changes in activity of excitable brain tissue; it is not a direct measure of neuronal activity. Fluctuations in regional neuronal activity can be inferred from the BOLD signal response. Neuronal activity requires energy, and it is currently thought that most of the energy demands of neurons is related to replenishment of postsynaptic neurotransmitters after neuronal firing.<sup>14</sup> Ultimately, the BOLD signal is more closely correlated with the relatively slowly fluctuating local field potential that represents the electrophysiological changes in groups of neurons, rather than the action potentials of individual neurons.<sup>36</sup>

Changes in CBF, CMRO<sub>2</sub> and cerebral blood volume (CBV) all contribute to a change in BOLD signal. An increase in CBF tends to increase BOLD signal, whilst an increase in CMRO<sub>2</sub> or CBV decreases BOLD signal.<sup>14</sup> Vasoactive stimuli, such as carbon dioxide, induce changes in BOLD signal by modifying CBF, to a first approximation, independently of neuronal stimuli.<sup>37</sup> BOLD fMRI has been widely used to infer changing neuronal activity in the brain but can also be useful in studying cerebral haemodynamics, as discussed below.

### Applications

Since its inception in the early 1990s,<sup>14</sup> BOLD fMRI has become the predominant MRI method of interrogating neural activity in the brain. Other non-invasive functional neuroimaging techniques such as electroencephalography (EEG) and magnetoencephalography (MEG) have a higher temporal resolution than BOLD. However, they are predominantly sensitive to cortical activity and have a low spatial resolution. BOLD can be used to probe whole-brain neural activity with a sub-millimetre resolution.

The increasing availability of 3 Tesla scanners in clinical practice, and the associated gain in signal-to-noise ratio and spatial resolution, has opened the door to the application of BOLD to study the brainstem.<sup>38</sup> BOLD has been applied to study regions of the brain involved in pain processing<sup>1,2</sup> including the midbrain neuronal response to visually triggered migraine.<sup>39</sup> The subcortical components of the default mode network (a network defined by coherent fluctuations of BOLD signal that appears active during wakeful rest) have been mapped using BOLD fMRI, including parts within the midbrain.<sup>4</sup> Brainstem neuronal activity in response to deep brain stimulation of the subthalamic nucleus (STN) in patients with Parkinson's disease has been demonstrated,<sup>40</sup> including recently in the intraoperative setting.<sup>41</sup> Several brainstem autonomic networks have

been mapped and studied, including those integral to regulation of systemic blood pressure<sup>5-7</sup> (Figure 4), respiration<sup>8,42</sup> and swallowing.<sup>43</sup> Visual processing networks in the brainstem have also been mapped.<sup>44</sup> BOLD EPI sequences are available for clinical scanners with which these techniques can be implemented. Whilst it is not currently feasible to diagnose network dysfunction in the individual patient, this might develop with higher field strengths (7T and beyond).

In the clinical setting, BOLD fMRI is used for presurgical planning to identify areas of functional activity that might be affected by surgery. Preoperative BOLD fMRI helps to guide the surgical approach and guide the use of intraoperative cortical stimulation in brain tumour surgery.<sup>45</sup> Brainstem tumours are more common in children than in adults and whilst some are treated surgically, they are often unresectable.<sup>46</sup> When surgical resection is attempted, diffusion tensor imaging (DTI), a microstructural technique that can be used to map the white matter tracts in the brainstem, has been shown to be useful in pre-operative planning<sup>47,48</sup> but it is not a reliable predictor of neurological deficits.<sup>48</sup> The development of brainstem BOLD could serve as an adjunct to DTI in pre-operative planning and potentially enable better predictions of neurological outcomes by accurately localising areas of important functional activity.

One limitation of the application and interpretation of BOLD fMRI in the clinical setting is the potential for decoupling of the neuronal and haemodynamic response. Brain pathology such as vascular malformations, areas of cerebral infarction or mass lesions can disrupt the mechanisms which underpin the BOLD response. This is especially problematic when BOLD fMRI is used for cortical mapping during surgery, where neurovascular uncoupling can lead to areas of false-negative BOLD response, potentially guiding the surgeon to unnecessarily resect areas of eloquent cortex.<sup>49</sup>

The acquisition of brainstem BOLD data necessitates physiological monitoring and correction, as discussed below. Despite these technical demands, brainstem BOLD does have potential as a clinical tool. Accurate functional localisation of brainstem nuclei could help in guiding placement of deep brain stimulators, as well as in guiding brainstem surgery to limit damage to important brainstem nuclei.

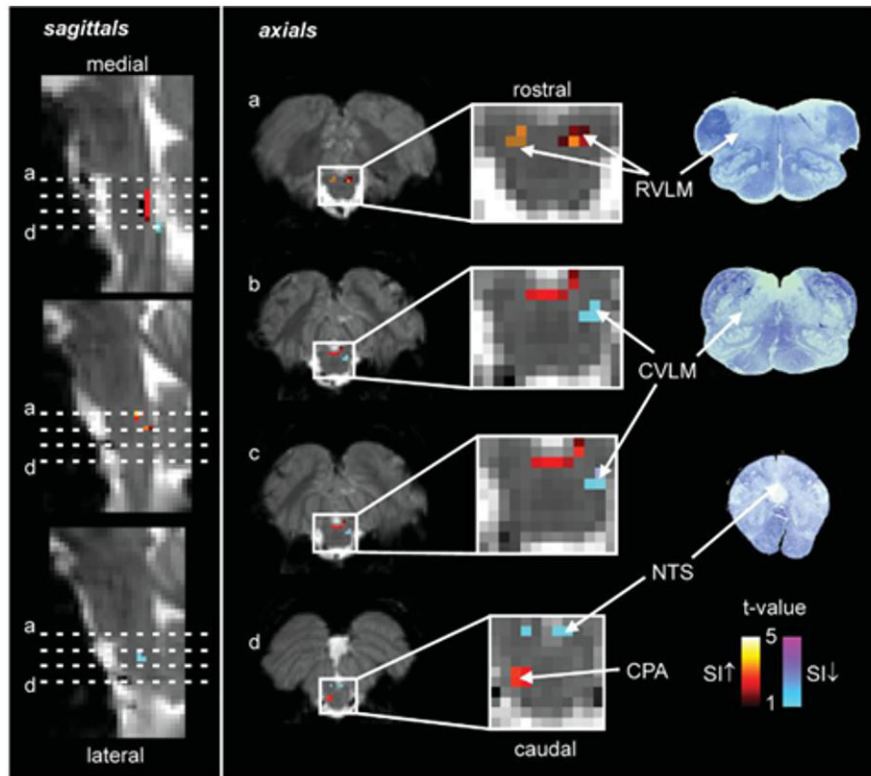
## CEREBROVASCULAR REACTIVITY

### Physical principles

CVR represents the capacity of a cerebral blood vessel to increase cerebral blood flow, via a change in vessel calibre, in response to a vasoactive stimulus. Measurement of CVR provides information on the functional vascular reserve, an important marker of the health of the cerebrovascular system.

In order to measure CVR, a vasoactive stimulus is administered and the cerebral blood flow response is measured. The most commonly applied vasoactive stimulus is carbon dioxide. When the arterial partial pressure of CO<sub>2</sub> (PaCO<sub>2</sub>) increases, CO<sub>2</sub> diffuses across the blood brain barrier<sup>50,51</sup> and causes hyperpolarisation of smooth muscle and endothelial cells. This results

Figure 4. Macefield *et al*<sup>6</sup> demonstrated functional activation in several medullary regions involved in autonomic supply to the cardiovascular system including the rostral ventrolateral medulla (RVLM), caudal ventrolateral medulla (CVLM), caudal pressor area (CPA) and nucleus tractus solitarius (NTS). Figure reproduced from 'Real-time imaging of the medullary circuitry involved in the generation of spontaneous muscle sympathetic nerve activity in awake subjects'<sup>6</sup> under Creative Commons Attribution 3.0 International License.



in smooth muscle relaxation and an increase in the release of endothelial factors such as nitric oxide, and subsequent vasodilation. Direct measurement of PaCO<sub>2</sub> is not possible using non-invasive methods. End-tidal CO<sub>2</sub> correlates with direct measurement of PaCO<sub>2</sub> via arterial blood gas sampling<sup>52</sup> and is therefore used as a surrogate marker of PaCO<sub>2</sub>.<sup>53</sup> Hypercapnia can be induced by administering a gas mixture containing 5% CO<sub>2</sub>, 21% O<sub>2</sub> and balanced nitrogen. Recently, computerised gas delivery systems have been developed that can prospectively target end-tidal CO<sub>2</sub><sup>54,55</sup> in an effort to standardise and improve repeatability of CVR measurements. However, specialist respiratory circuits are not a prerequisite to CVR measurement. Hypercapnia can be induced as simply as through a breath-hold, with ETCO<sub>2</sub> measured via nasal cannulae.

The response to vasoactive simulation can be measured using a variety of methods. These include transcranial Doppler ultrasound measurement of the change in blood velocity and vessel diameter, and phase-contrast MRI, but both of these techniques are limited to assessing CVR in individual arterial territories,<sup>56,57</sup> unlike ASL or BOLD fMRI that can map across the whole brain. CVR measurements require at least two estimates of CBF. MRI, therefore, offers an advantage over PET, SPECT and CT<sup>58,59</sup> in that it does not require the use of ionising radiation. In the research setting, the majority of CVR studies are based on BOLD MRI,<sup>59</sup> because of its widespread availability, high sensitivity, and

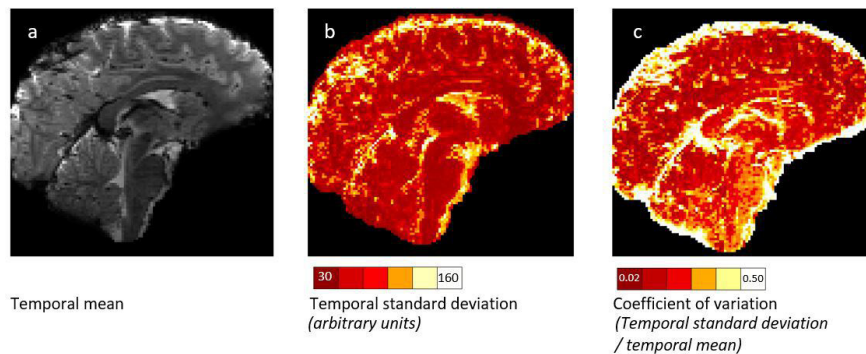
high spatial and temporal resolution.<sup>60</sup> However, BOLD is not a specific measure of cerebral blood flow<sup>61</sup> and therefore only provides a semi-quantitative measurement of CVR. BOLD-CVR and ASL-CVR are generally in good agreement with each other,<sup>59</sup> but ASL has the advantage of providing a quantifiable measure of CBF,<sup>62</sup> with the caveat that the contrast to noise ratio (CNR) for detecting changes in CBF is typically lower than BOLD.

In order to calculate CVR, the BOLD or ASL signal is measured at the subject's baseline end-tidal CO<sub>2</sub> and during hypercapnia. The proportional BOLD or CBF response is then calculated and expressed as either a percentage change in BOLD signal or a percentage change in CBF per mmHg increase in end-tidal CO<sub>2</sub>.

#### Applications

CVR correlates with angiographic measures of disease severity both in atherosclerotic and Moyamoya patients<sup>63</sup> and could therefore serve as an adjunct to angiography in selecting patients for revascularisation therapy. Measurement of CVR could also help in the assessment of the rehabilitation potential of brain regions affected by ischaemic stroke.<sup>64</sup> CVR could be useful as a marker of neurovascular reserve in a variety of cerebrovascular diseases. For example, CVR measurements correlate with cognitive performance in patients with mild cognitive decline<sup>65,66</sup> with the severity of regional arterial stenosis in Moyamoya,<sup>67</sup> and with the severity of motor symptoms in Parkinson's disease.<sup>68</sup>

Figure 5. Temporal mean (a), temporal standard deviation (b) and coefficient of variation (c) of a 7T resting state BOLD fMRI acquisition demonstrates the high temporal variance in resting state fMRI signal in the brainstem and surrounding structures.



The assessment of brainstem CVR could be useful in pre-surgical planning when the neurovascular coupling that underpins the BOLD signal response is compromised by brain pathology. For example, Pillai et al demonstrated that low-grade gliomas can have preserved cerebral blood flow but impaired CVR, thus impeding evaluation of functional activity adjacent to the tumour due to the resultant neurovascular uncoupling<sup>49,69</sup> This additional knowledge on the state of the local vasculature may help determine the necessity of intra-operative cortical mapping. BOLD-CVR has also been used intraoperatively to determine whether there has been an immediate improvement in cerebral haemodynamics following arterial bypass graft surgery.<sup>70</sup> The same technique has also been applied to assess CVR following tumour resection, and areas of impaired CVR have been shown to correlate with tumour recurrence on subsequent post-operative contrast-enhanced  $T_1$ -weighted scans.<sup>70</sup>

CVR measurements are reproducible using both 1.5T and 3T MRI<sup>71,72</sup> and are safe and well-tolerated in the clinical population using a  $\text{CO}_2$  stimulus and BOLD MRI acquisition.<sup>73</sup> Brainstem ASL-CVR and BOLD-CVR measurements are both feasible at 3T.<sup>62</sup> Sleight et al's comprehensive review of CVR measurement approaches could serve as a foundation for the application of CVR as a clinical tool.<sup>74</sup>

#### CHALLENGES OF BRAINSTEM FUNCTIONAL MRI

The application of the above techniques in the brainstem is challenging for several reasons. Achieving sufficient signal-to-noise (SNR) and thus spatial resolution to image the sub-millimetre internal architecture of the brainstem is time-consuming.<sup>75</sup> However, the move towards higher MRI field strengths, 3T in the clinical environment and 7T largely as a research tool, helps to address this problem. The brainstem's caudal location places it away from the elements of typical MRI receiver head coils, further compromising SNR. The susceptibility-induced gradient in the static magnetic field of the scanner caused by air-tissue interfaces in the nearby paranasal sinuses causes distortions and signal drop out.<sup>76</sup> Gradient-echo echo planar imaging (GE-EPI) is almost ubiquitous for BOLD fMRI and is commonly used for ASL, but it is especially vulnerable to such artefacts.<sup>77</sup> For ASL in particular, these problems can be partially addressed using alternative readouts such as 3D spiral,<sup>78</sup> together with parallel imaging,

which reduces image acquisition time and susceptibility-induced distortion.<sup>77</sup>

The brainstem is especially subject to physiological noise (Figure 5). The change in the volume and position of the lungs during respiration causes fluctuations in the static magnetic field present at the brainstem.<sup>79</sup> This causes misregistration of MRI signal and subsequent anatomic distortion. This effect decreases with the cube of the distance from the lungs, and therefore the brainstem is more strongly affected than the cerebral hemispheres.<sup>75</sup> Head movement, physiological tissue displacements due to pressure pulsations from the adjacent vertebralbasilar artery or CSF pulsation can cause BOLD and ASL artefacts and misalignment of ASL tag-control volumes.<sup>80,81</sup> The brainstem is especially vulnerable to physiological pulsations; motion of structures across the cardiac cycle are of the order of 0.5 mm close to the brainstem compared to 0.05 mm in the cerebral cortex.<sup>82,83</sup>

Moving towards higher static magnetic fields can increase SNR which can be traded for an increase in spatial resolution which is necessary to better resolve brainstem nuclei. However, the stronger static magnetic field may introduce problems of its own. These include less uniform transmit and receive radiofrequency fields,<sup>84</sup> stronger field gradients at air-tissue interfaces exacerbating susceptibility-induced artefacts<sup>84,85</sup> and increased soft tissue energy deposition<sup>85</sup> associated with the higher Larmor frequency. Furthermore, physiological noise is proportional to the square of the magnetic field strength.<sup>77</sup> Physiological noise can be addressed prospectively using navigator methods which track brain motion during the MRI acquisition<sup>86</sup> or through cardiac gating.<sup>81</sup> Alternatively, physiological parameters such as heart and respiratory rate can be recorded using physiological monitoring and a retrospective correction applied<sup>87</sup> or data-driven methods may be applied based on the spatio-temporal characteristics of physiological noise.<sup>77</sup> Applying a brainstem mask to remove areas of high physiological noise such as the surrounding CSF and vascular spaces can also improve sensitivity to detect functional activity.<sup>88</sup> Anatomical identification of brainstem nuclei to aid functional localisation is also challenging, although techniques such as magnetisation transfer imaging have been used to identify certain brainstem nuclei.<sup>89</sup>

## CONCLUSION

Despite the above challenges, functional MRI techniques based on ASL and BOLD can be used to non-invasively investigate neuronal activity and cerebral haemodynamics across the brain. They have been applied to study a variety of disease processes and are already used in certain clinical circumstances. Brainstem functional MRI is challenging, but with further optimisation could feasibly be applied in the clinical setting. Many of the techniques described in this review are feasible in the brainstem using existing 3 Tesla scanners,

which are increasingly prevalent in the clinical setting. At 3T, ASL could be applied to map brainstem perfusion in acute ischaemic stroke, as well as estimating brainstem tumour haemodynamics to guide diagnosis and to assess response to treatment. CVR could be useful as a prognostication tool when brainstem haemodynamics are compromised. Finally, higher field strength scanners may render methods such as the mapping of brainstem neural networks using BOLD interpretable at an individual level.

## REFERENCES

- Robertson RV, Crawford LS, Meylakh N, Macey PM, Macefield VG, Keay KA, et al. Regional hypothalamic, amygdala, and midbrain periaqueductal gray matter recruitment during acute pain in awake humans: A 7-Tesla functional magnetic resonance imaging study. *Neuroimage* 2022; **259**: S1053-8119(22)00525-0. <https://doi.org/10.1016/j.neuroimage.2022.119408>
- Staud R, Boissoneault J, Lai S, Mejia MS, Ramanlal R, Godfrey MM, et al. Spinal cord neural activity of patients with fibromyalgia and healthy controls during temporal summation of pain: an fMRI study. *J Neurophysiol* 2021; **126**: 946–56. <https://doi.org/10.1152/jn.00276.2021>
- Gili T, Saxena N, Diukova A, Murphy K, Hall JE, Wise RG. The thalamus and brainstem act as key hubs in alterations of human brain network connectivity induced by mild propofol sedation. *J Neurosci* 2013; **33**: 4024–31. <https://doi.org/10.1523/JNEUROSCI.3480-12.2013>
- Li J, Curley WH, Guerin B, Dougherty DD, Dalca AV, Fischl B, et al. Mapping the subcortical connectivity of the human default mode network. *Neuroimage* 2021. <https://doi.org/10.1101/2021.07.13.452265>
- Lundblad LC, Fatouleh RH, Hammam E, McKenzie DK, Macefield VG, Henderson LA. Brainstem changes associated with increased muscle sympathetic drive in obstructive sleep apnoea. *NeuroImage* 2014; **103**: 258–66. <https://doi.org/10.1016/j.neuroimage.2014.09.031>
- Macefield VG, Henderson LA. Real-time imaging of the medullary circuitry involved in the generation of spontaneous muscle sympathetic nerve activity in awake subjects. *Hum Brain Mapp* 2010; **31**: 539–49. <https://doi.org/10.1002/hbm.20885>
- Coulson JM, Murphy K, Harris AD, Fjodorova M, Cockcroft JR, Wise RG. Correlation between baseline blood pressure and the brainstem response to isometric forearm contraction in human volunteers: a pilot study. *J Hum Hypertens* 2015; **29**: 449–55. <https://doi.org/10.1038/jhh.2014.103>
- Pattinson KTS, Mitsis GD, Harvey AK, Jbabdi S, Dirckx S, Mayhew SD, et al. Determination of the human brainstem respiratory control network and its cortical connections in vivo using functional and structural imaging. *Neuroimage* 2009; **44**: 295–305. <https://doi.org/10.1016/j.neuroimage.2008.09.007>
- Luft AR, Skalej M, Schulz JB, Welte D, Kolb R, Bürk K, et al. Patterns of age-related shrinkage in cerebellum and brainstem observed in vivo using three-dimensional MRI Volumetry. *Cereb Cortex* 1999; **9**: 712–21. <https://doi.org/10.1093/cercor/9.7.712>
- Raininko R, Autti T, Vanhanen SL, Ylikoski A, Erkinjuntti T, Santavuori P. The normal brain stem from infancy to old age - A morphometric MRI study. *Neuroradiology* 1994; **36**: 364–68. <https://doi.org/10.1007/BF00612119>
- Naidich TP, Duvernoy HM, Delman BN, Sorensen AG, Kollias SS, Haacke EM. Duvernoy's Atlas of the Human Brain Stem and Cerebellum. In: *Duvernoy's Atlas of the Human Brain Stem and Cerebellum*. Vienna: Springer; 2009. <https://doi.org/10.1007/978-3-211-73971-6>
- Shah A, Jhavar SS, Nunez M, Goel A, Goel A. Brainstem anatomy: A study on the basis of the pattern of fiber organization. *World Neurosurg* 2020; **134**: e826–46. <https://doi.org/10.1016/j.wneu.2019.11.016>
- Akar ZC, Dujovny M, Slavin KV, Gomez-Tortosa E, Ausman JI. Microsurgical anatomy of the intracranial part of the vertebral artery. *Neurological Research* 1994; **16**: 171–80. <https://doi.org/10.1080/01616412.1994.11740221>
- Buxton RB. Introduction to Functional Magnetic Resonance Imaging. In: *Introduction to Functional Magnetic Resonance Imaging: Principles and Techniques*. Cambridge University Press; 2002. <https://doi.org/10.1017/CBO9780511549854>
- Alsop DC, Detre JA, Golay X, Günther M, Hendrikse J, Hernandez-Garcia L, et al. Recommended implementation of arterial spin-labelled perfusion MRI for clinical applications: A consensus of the ISMRM perfusion study group and the European consortium for ASL in dementia. *Magn Reson Med* 2015; **73**: 102–16. <https://doi.org/10.1002/mrm.25197>
- Golay X, Mai-Lan H. Multidelay ASL of the pediatric brain. *The British Journal of Radiology* 2022.
- Wong EC, Cronin M, Wu W-C, Inglis B, Frank LR, Liu TT. Velocity-selective arterial spin labeling. *Magn Reson Med* 2006; **55**: 1334–41. <https://doi.org/10.1002/mrm.20906>
- Wu W-C, Wong EC. Intravascular effect in velocity-selective arterial spin labeling: the choice of inflow time and cutoff velocity. *Neuroimage* 2006; **32**: 122–28. <https://doi.org/10.1016/j.neuroimage.2006.03.001>
- Grade M, Hernandez Tamames JA, Pizzini FB, Achten E, Golay X, Smits M. A Neuroradiologist's guide to arterial spin labeling MRI. *Neuroradiology* 2015; **57**: 1181–1202. <https://doi.org/10.1007/s00234-015-1571-z>
- Al-Bachari S, Parkes LM, Vidyasagar R, Hanby MF, Tharaken V, Leroi I, et al. Arterial spin labelling reveals prolonged arterial arrival time in idiopathic Parkinson's disease. *Neuroimage Clin* 2014; **6**: 1–8. <https://doi.org/10.1016/j.nicl.2014.07.014>
- Johnston ME, Lu K, Maldjian JA, Jung Y. Multi-TI arterial spin labeling MRI with variable TR and bolus duration for cerebral blood flow and arterial transit time mapping. *IEEE Trans Med Imaging* 2015; **34**: 1392–1402. <https://doi.org/10.1109/TMI.2015.2395257>



22. Srinivasan A, Goyal M, Al Azri F, Lum C. State-of-the-art imaging of acute stroke. *Radiographics* 2006; **26 Suppl 1**: S75–95. <https://doi.org/10.1148/rg.26si065501>
23. Lindner T, Bolar DS, Achten E, Barkhof F, Bastos-Leite AJ, Detre JA, et al. Current state and guidance on arterial spin labeling perfusion MRI in clinical imaging. *Magn Reson Med* 2023; **89**: 2024–47. <https://doi.org/10.1002/mrm.29572>
24. Wang DJJ, Alger JR, Qiao JX, Hao Q, Hou S, Fiaz R, et al. The value of arterial spin-labeled perfusion imaging in acute ischemic stroke – comparison with dynamic susceptibility contrast enhanced MRI. *Stroke* 2012; **43**: 1018–24. <https://doi.org/10.1161/STROKEAHA.111.631929>
25. Bokkers RPH, Hernandez DA, Merino JG, Mirasol RV, van Osch MJ, Hendrikse J, et al. Whole-brain arterial spin labeling perfusion MRI in patients with acute stroke. *Stroke* 2012; **43**: 1290–94. <https://doi.org/10.1161/STROKEAHA.110.589234>
26. Haller S, Zaharchuk G, Thomas DL, Lovblad K-O, Barkhof F, Golay X. Arterial spin labeling perfusion of the brain: emerging clinical applications. *Radiology* 2016; **281**: 337–56. <https://doi.org/10.1148/radiol.2016150789>
27. Manning P, Daghighi S, Rajaratnam MK, Parthiban S, Bahrami N, Dale AM, et al. Differentiation of progressive disease from pseudoprogression using 3D PCASL and DSC perfusion MRI in patients with glioblastoma. *J Neurooncol* 2020; **147**: 681–90. <https://doi.org/10.1007/s11060-020-03475-y>
28. Gulani V, Calamante F, Shellock FG, Kanal E, Reeder SB, International Society for Magnetic Resonance in Medicine. Gadolinium deposition in the brain: summary of evidence and recommendations. *Lancet Neurol* 2017; **16**: 564–70. [https://doi.org/10.1016/S1474-4422\(17\)30158-8](https://doi.org/10.1016/S1474-4422(17)30158-8)
29. Buxton RB, Frank LR. A model for the coupling between cerebral blood flow and oxygen metabolism during neural stimulation. *J Cereb Blood Flow Metab* 1997; **17**: 64–72. <https://doi.org/10.1097/00004647-199701000-00009>
30. Pizzini Fet al. Cerebral perfusion alterations in epileptic patients during peri-ictal and post-ictal phase: PASL vs DSC-MRI. *Magn Resonance Imaging* 2013; 1001–5.
31. Marquand AF, O'Daly OG, De Simoni S, Alsop DC, Maguire RP, Williams SCR, et al. Dissociable effects of methylphenidate, atomoxetine and placebo on regional cerebral blood flow in healthy volunteers at rest: a multi-class pattern recognition approach. *Neuroimage* 2012; **60**: 1015–24. <https://doi.org/10.1016/j.neuroimage.2012.01.058>
32. Wang J, Li J, Yin X, Zhou H, Zheng Y, Liu H. Cerebral hemodynamics of hypoxic-ischemic encephalopathy neonates at different ages detected by arterial spin labeling imaging. *Clin Hemorheol Microcirc* 2022; **81**: 271–79. <https://doi.org/10.3233/CH-211324>
33. Zheng Q, Freeman CW, Hwang M. Sex-related differences in arterial spin-labelled perfusion of metabolically active brain structures in neonatal hypoxic-ischaemic encephalopathy. *Clin Radiol* 2021; **76**: S0009-9260(21)00029-5: 342–47. <https://doi.org/10.1016/j.crad.2020.12.026>
34. Xing W, Wang X, Liao X, Liao W, Shen L. Spin labeling artery method perfusion MRI study of SPG4 and SCA3/MJD. *Magn Reson Imaging* 2014; **32**: S0730-725X(14)00253-7: 1330–34. <https://doi.org/10.1016/j.mri.2014.08.022>
35. Phillips AA, Chan FH, Zheng MMZ, Krassioukov AV, Ainslie PN. Neurovascular coupling in humans: physiology, methodological advances and clinical implications. *J Cereb Blood Flow Metab* 2016; **36**: 647–64. <https://doi.org/10.1177/0271678X15617954>
36. Logothetis NK. The neural basis of the blood-oxygen-level-dependent functional magnetic resonance imaging signal. *Philos Trans R Soc Lond B Biol Sci* 2002; **357**: 1003–37. <https://doi.org/10.1098/rstb.2002.1114>
37. Davis TL, Kwong KK, Weisskoff RM, Rosen BR. Calibrated functional MRI: mapping the dynamics of oxidative metabolism. *Proc Natl Acad Sci U S A* 1998; **95**: 1834–39. <https://doi.org/10.1073/pnas.95.4.1834>
38. Hahn A, Kranz GS, Seidel E-M, Sladky R, Kraus C, Küblböck M, et al. Comparing neural response to painful electrical stimulation with functional MRI at 3 and 7 T. *Neuroimage* 2013; **82**: 336–43. <https://doi.org/10.1016/j.neuroimage.2013.06.010>
39. Cao Y, Aurora SK, Nagesh V, Patel SC, Welch KMA. Functional MRI-BOLD of brainstem structures during visually triggered migraine. *Neurology* 2002; **59**: 72–78. <https://doi.org/10.1212/wnl.59.1.72>
40. Stefurak T, Mikulis D, Mayberg H, Lang AE, Hevenor S, Pahapill P, et al. Deep brain stimulation for Parkinson's disease dissociates mood and motor circuits: a functional MRI case study. *Mov Disord* 2003; **18**: 1508–16. <https://doi.org/10.1002/mds.10593>
41. Gibson W. Symptom-specific differential motor network modulation by deep brain stimulation in Parkinson's disease. *J Neurosurgery* 2021; 1–9.
42. McKay LC, Adams L, Frackowiak RSJ, Corfield DR. A bilateral cortico-bulbar network associated with breath holding in humans, determined by functional magnetic resonance imaging. *Neuroimage* 2008; **40**: 1824–32. <https://doi.org/10.1016/j.neuroimage.2008.01.058>
43. Hartnick CJ, Rudolph C, Willging JP, Holland SK. Functional magnetic resonance imaging of the pediatric swallow: imaging the cortex and the brainstem. *Laryngoscope* 2001; **111**: 1183–91. <https://doi.org/10.1097/00005537-200107000-00010>
44. Wildenberg JC, Tyler ME, Danilov YP, Kaczmarek KA, Meyerand ME. High-resolution fMRI detects neuromodulation of individual brainstem nuclei by electrical tongue stimulation in balance-impaired individuals. *Neuroimage* 2011; **56**: 2129–37. <https://doi.org/10.1016/j.neuroimage.2011.03.074>
45. Zaca D, Hua J, Pillai JJ. Cerebrovascular reactivity mapping for brain tumor presurgical planning. *World J Clin Oncol* 2011; **2**: 289–98. <https://doi.org/10.5306/wjco.v2.i7.289>
46. Eisele SC, Reardon DA. Adult brainstem gliomas. *Cancer* 2016; **122**: 2799–2809. <https://doi.org/10.1002/cncr.29920>
47. Xiao X, Kong L, Pan C, Zhang P, Chen X, Sun T, et al. The role of diffusion tensor imaging and tractography in the surgical management of brainstem gliomas. *Neurosurg Focus* 2021; **50**: 2020.10. FOCUS20166. <https://doi.org/10.3171/2020.10.FOCUS20166>
48. Rogalska M, Antkowiak L, Mandera M. Clinical application of diffusion tensor imaging and fiber tractography in the management of brainstem cavernous malformations: a systematic review. *Neurosurg Rev* 2022; **45**: 2027–40. <https://doi.org/10.1007/s10143-022-01759-7>
49. Pillai JJ, Mikulis DJ. Cerebrovascular reactivity mapping: an evolving standard for clinical functional imaging. *AJNR Am J Neuroradiol* 2015; **36**: 7–13. <https://doi.org/10.3174/ajnr.A3941>
50. Willie CK, Tzeng Y-C, Fisher JA, Ainslie PN. Integrative regulation of human brain blood flow. *J Physiol* 2014; **592**: 841–59. <https://doi.org/10.1113/jphysiol.2013.268953>
51. Liu P, De Vis JB, Lu H. Cerebrovascular reactivity (CVR) MRI with CO2 challenge: A technical review. *Neuroimage* 2019; **187**: S1053-8119(18)30257-X: 104–15. <https://doi.org/10.1016/j.neuroimage.2018.03.047>
52. Razi E, Moosavi GA, Omidi K, Khakpour Saebi A, Razi A. Correlation of end-tidal carbon dioxide with arterial carbon dioxide in mechanically ventilated patients. *Arch*

- Trauma Res* 2012; **1**: 58–62. <https://doi.org/10.5812/at.6444>
53. Hemmati Net al. Correlation between end-tidal and arterial carbon dioxide partial pressure in patients undergoing craniotomy. *J Inj Violence Res* 2012.
  54. Fisher JA. The CO<sub>2</sub> stimulus for cerebrovascular reactivity: fixing inspired concentrations vs. targeting end-tidal partial pressures. *J Cereb Blood Flow Metab* 2016; **36**: 1004–11. <https://doi.org/10.1177/0271678X16639326>
  55. Whittaker JR, Driver ID, Bright MG, Murphy K. The absolute CBF response to activation is preserved during elevated perfusion: implications for neurovascular coupling measures. *Neuroimage* 2016; **125**: 198–207. <https://doi.org/10.1016/j.neuroimage.2015.10.023>
  56. McDonnell MN, Berry NM, Cutting MA, Keage HA, Buckley JD, Howe PRC. Transcranial Doppler ultrasound to assess cerebrovascular reactivity: reliability, reproducibility and effect of posture. *PeerJ* 2013; **1**: e65. <https://doi.org/10.7717/peerj.65>
  57. Skow RJ, MacKay CM, Tymko MM, Willie CK, Smith KJ, Ainslie PN, et al. Differential cerebrovascular CO<sub>2</sub> reactivity in anterior and posterior cerebral Circulations. *Respir Physiol Neurobiol* 2013; **189**: 76–86. <https://doi.org/10.1016/j.resp.2013.05.036>
  58. Endo H, Inoue T, Ogasawara K, Fukuda T, Kanbara Y, Ogawa A. Quantitative assessment of cerebral hemodynamics using perfusion-weighted MRI in patients with major cerebral artery occlusive disease. *Stroke* 2006; **37**: 388–92. <https://doi.org/10.1161/01.STR.0000199030.37274.88>
  59. Sleight E, Stringer MS, Marshall I, Wardlaw JM, Thrippleton MJ. Cerebrovascular reactivity measurement using magnetic resonance imaging: A systematic review. *Front Physiol* 2021; **12**: 643468. <https://doi.org/10.3389/fphys.2021.643468>
  60. Taneja K, Liu P, Xu C, Turner M, Zhao Y, Abdelkarim D, et al. Quantitative cerebrovascular reactivity in normal aging: comparison between phase-contrast and arterial spin labeling MRI. *Front Neurol* 2020; **11**: 758. <https://doi.org/10.3389/fneur.2020.00758>
  61. Arthurs OJ, Boniface S. How well do we understand the neural origins of the fMRI BOLD signal *Trends Neurosci* 2002; **25**: 27–31. [https://doi.org/10.1016/s0166-2236\(00\)01995-0](https://doi.org/10.1016/s0166-2236(00)01995-0)
  62. Warnert EAH, Harris AD, Murphy K, Saxena N, Tailor N, Jenkins NS, et al. In vivo assessment of human brainstem cerebrovascular function: a multi-inversion time pulsed arterial spin labelling study. *J Cereb Blood Flow Metab* 2014; **34**: 956–63. <https://doi.org/10.1038/jcbfm.2014.39>
  63. Donahue MJ, Dethrage LM, Faraco CC, Jordan LC, Clemmons P, Singer R, et al. Routine clinical evaluation of cerebrovascular reserve capacity using carbogen in patients with intracranial stenosis. *Stroke* 2014; **45**: 2335–41. <https://doi.org/10.1161/STROKEAHA.114.005975>
  64. Krishnamurthy V, Sprick JD, Krishnamurthy LC, Barter JD, Turabi A, Hajjar IM, et al. The utility of cerebrovascular reactivity MRI in brain rehabilitation: A mechanistic perspective. *Front Physiol* 2021; **12**: 642850. <https://doi.org/10.3389/fphys.2021.642850>
  65. Richiardi J, Monsch AU, Haas T, Barkhof F, Van de Ville D, Radü EW, et al. Altered cerebrovascular reactivity velocity in mild cognitive impairment and Alzheimer's disease. *Neurobiol Aging* 2015; **36**: 33–41. <https://doi.org/10.1016/j.neurobiolaging.2014.07.020>
  66. Kim D, Hughes TM, Lipford ME, Craft S, Baker LD, Lockhart SN, et al. Relationship between cerebrovascular reactivity and cognition among people with risk of cognitive decline. *Front Physiol* 2021; **12**: 645342. <https://doi.org/10.3389/fphys.2021.645342>
  67. Federau C, Christensen S, Zun Z, Park S-W, Ni W, Moseley M, et al. Cerebral blood flow, transit time, and apparent diffusion coefficient in Moyamoya disease before and after acetazolamide. *Neuroradiology* 2017; **59**: 5–12. <https://doi.org/10.1007/s00234-016-1766-y>
  68. Pelizzari L, Laganà MM, Rossetto F, Bergsland N, Galli M, Baselli G, et al. Cerebral blood flow and cerebrovascular reactivity correlate with severity of motor symptoms in Parkinson's disease. *Ther Adv Neurol Disord* 2019; **12**: 1756286419838354. <https://doi.org/10.1177/1756286419838354>
  69. Pillai JJ, Zacá D. Clinical utility of cerebrovascular reactivity mapping in patients with low grade gliomas. *World J Clin Oncol* 2011; **2**: 397–403. <https://doi.org/10.5306/wjco.v2.i12.397>
  70. Muscas GRecent Advances and Future Directions: Clinical Applications of Intraoperative BOLD-MRI CVR. In: *In Chen Jea. Cerebrovascular Reactivity. Neuromethods*. New York, NY: Humana; 2022. <https://doi.org/10.1007/978-1-0716-1763-2>
  71. Stringer MS, Blair GW, Shi Y, Hamilton I, Dickie DA, Doubal FN, et al. A comparison of CVR magnitude and delay assessed at 1.5 and 3T in patients with cerebral small vessel disease. *Front Physiol* 2021; **12**: 644837. <https://doi.org/10.3389/fphys.2021.644837>
  72. Thrippleton MJ, Shi Y, Blair G, Hamilton I, Waiter G, Schwarzbauer C, et al. Cerebrovascular reactivity measurement in cerebral small vessel disease: rationale and reproducibility of a protocol for MRI acquisition and image processing. *Int J Stroke* 2018; **13**: 195–206. <https://doi.org/10.1177/1747493017730740>
  73. Spano VR, Mandell DM, Poulblanc J, Sam K, Battisti-Charbonney A, Pucci O, et al. CO<sub>2</sub> blood oxygen level-dependent MR mapping of cerebrovascular reserve in a clinical population: safety, tolerability, and technical feasibility. *Radiology* 2013; **266**: 592–98. <https://doi.org/10.1148/radiol.12112795>
  74. Sleight E, Stringer MS, Marshall I, Wardlaw JM, Thrippleton MJ. Cerebrovascular reactivity measurement using magnetic resonance imaging: A systematic review. *Front Physiol* 2021; **12**: <https://doi.org/10.3389/fphys.2021.643468>
  75. Sclocco R, Beissner F, Bianciardi M, Polimeni JR, Napadow V. Challenges and opportunities for brainstem neuroimaging with ultrahigh field MRI. *Neuroimage* 2018; **168**: S1053-8119(17)30163-5: 412–26. <https://doi.org/10.1016/j.neuroimage.2017.02.052>
  76. Glover GH, Law CS. Spiral-in/out BOLD fMRI for increased SNR and reduced susceptibility artifacts. *Magn Reson Med* 2001; **46**: 515–22. <https://doi.org/10.1002/mrm.1222>
  77. Brooks JCW, Faull OK, Pattinson KTS, Jenkinson M. Physiological noise in brainstem fMRI. *Front Hum Neurosci* 2013; **7**: <https://doi.org/10.3389/fnhum.2013.00623>
  78. Block KT, Chandarana H, Milla S, Bruno M, Mulholland T, Fatterpekar G, et al. Toward routine clinical use of radial stack-of-stars 3D gradient-echo sequences for reducing motion sensitivity. *J Korean Soc Magn Reson Med* 2014; **18**: 87. <https://doi.org/10.13104/jksmrm.2014.18.2.87>
  79. Raj D, Paley DP, Anderson AW, Kennan RP, Gore JC. A model for susceptibility artefacts from respiration in functional echo-planar magnetic resonance imaging. *Phys Med Biol* 2000; **45**: 3809–20. <https://doi.org/10.1088/0031-9155/45/12/321>
  80. Sweetman B, Linninger AA. Cerebrospinal fluid flow dynamics in the central nervous system. *Ann Biomed Eng* 2011; **39**: 484–96. <https://doi.org/10.1007/s10439-010-0141-0>
  81. Beissner F. Functional MRI of the brainstem: common problems and their solutions. *Clin Neuroradiol* 2015; **25 Suppl 2**: 251–57. <https://doi.org/10.1007/s00062-015-0404-0>
  82. Harvey AK, Pattinson KTS, Brooks JCW, Mayhew SD, Jenkinson M, Wise RG. Brainstem functional magnetic resonance

- imaging: disentangling signal from physiological noise. *J Magn Reson Imaging* 2008; **28**: 1337–44. <https://doi.org/10.1002/jmri.21623>
83. Enzmann DR, Pelc NJ. Brain motion: measurement with phase-contrast MR imaging. *Radiology* 1992; **185**: 653–60. <https://doi.org/10.1148/radiology.185.3.1438741>
84. Ladd ME, Bachert P, Meyerspeer M, Moser E, Nagel AM, Norris DG, et al. Pros and cons of ultra-high-field MRI/MRS for human application. *Prog Nucl Magn Reson Spectrosc* 2018; **109**: 1–50. <https://doi.org/10.1016/j.pnmrs.2018.06.001>
85. Oliveira ÍAF, Roos T, Dumoulin SO, Siero JCW, van der Zwaag W. Can 7T MPRAGE match MP2RAGE for gray-white matter contrast? *Neuroimage*. *Neuroimage* 2021; **240**: S1053-8119(21)00660-1. <https://doi.org/10.1016/j.neuroimage.2021.118384>
86. Hu X, Kim SG. Reduction of signal fluctuation in functional MRI using navigator echoes. *Magn Reson Med* 1994; **31**: 495–503. <https://doi.org/10.1002/mrm.1910310505>
87. Glover GH, Li T-Q, Ress D. Image-based method for retrospective correction of physiological motion effects in fMRI: RETROICOR. *Magn Reson Med* 2000; **44**: 162–67. [https://doi.org/10.1002/1522-2594\(200007\)44:1<162::AID-MRM23>3.0.CO;2-E](https://doi.org/10.1002/1522-2594(200007)44:1<162::AID-MRM23>3.0.CO;2-E)
88. Beissner F, Schumann A, Brunn F, Eisenträger D, Bär K-J. Advances in functional magnetic resonance imaging of the human brainstem. *Neuroimage* 2014; **86**: 91–98. <https://doi.org/10.1016/j.neuroimage.2013.07.081>
89. Liu KY, Marijatta F, Hämmerer D, Acosta-Cabronero J, Düzel E, Howard RJ. Magnetic resonance imaging of the human locus coeruleus: A systematic review. *Neurosci Biobehav Rev* 2017; **83**: 325–55. <https://doi.org/10.1016/j.neubiorev.2017.10.023>